ACS Catalysis

Research Article

Cite This: ACS Catal. 2018, 8, 837−844

pubs.acs.org/acscatalysis

Sulfur-Modified Copper Catalysts for the Electrochemical Reduction of Carbon Dioxide to Formate

Tatsuya Shinagawa,[†] Gastón O. Larrazábal,[†] Antonio J. Martín,[†] Frank Krumeich,[§] and Javier Pérez-Ramírez*[,†]

[†]Institute for Chemical and Bioengineering, Department of Chemistry and Applied Biosciences, ETH Zurich, Vladimir-Prelog-Weg 1, 8093 Zurich, Switzerland

[§]Laboratory of Inorganic Chemistry, Department of Chemistry and Applied Biosciences, ETH Zurich, Vladimir-Prelog-Weg 1, 8093 Zurich, Switzerland

Supporting Information

ABSTRACT: The electrocatalytic CO_2 reduction reaction (eCO_2RR) has been gaining increasing attention owing to its potential to contribute to sustainability in our society, although enhanced catalytic performance is a prerequisite for its implementation. Herein, Cu electrocatalysts modified with sulfur proved to selectively produce formate via aqueous eCO_2RR and thus to unexpectedly prevent the mechanistic fingerprint of Cu (i.e., the CO path). Initially, sulfur-modified copper catalysts (Cu−S) were prepared by the in situ reductive reconstruction of nano CuS precursors, revealing a positive correlation between particle size and selectivity toward formate. Subsequent studies over targeted submicron Cu−S particles with varying sulfur content demonstrated their evolution under reaction conditions, attaining a similar surface state comprising metallic Cu and sulfide phases, irrespective of the initial structure of the materials. In accordance, the initial sulfur content showed only a very limited influence on the catalytic performance, which remained at approximately 80% Faradaic efficiency toward formate at −0.8 V vs RHE, outperforming all cost-effective, earth-abundant, and nontoxic electrocatalysts reported to date for the production of formate via the aqueous eCO_2RR.

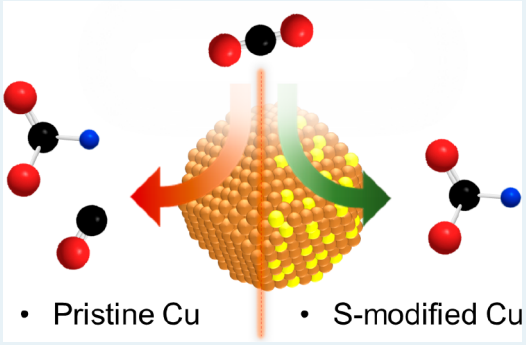

KEYWORDS: *electrocatalysis, CO_2 reduction, formate, copper, sulfide*

1. INTRODUCTION

The conversion of H_2O and CO_2 into fuels and value-added compounds in combination with renewable energy sources may effectively contribute to establishing a more sustainable circulation of energy and materials.[1,2] In this context, the electrocatalytic CO_2 reduction reaction (eCO_2RR) has been attracting increasing attention, owing to its potential contribution to closing the carbon cycle.[3−6]

Since the pioneering works of Hori and co-workers,[3,7,8] a number of materials have been examined as catalysts for the eCO_2RR in aqueous media.[6] Among the eCO_2RR-active metal electrodes, gold and silver are known for their comparatively high activity toward CO,[8] whereas palladium and some p-block elements, such as tin and indium, direct the reaction toward the production of formate.[8] Copper electrodes are unique due to the production of highly reduced compounds, such as hydrocarbons and alcohols, in appreciable amounts at high overpotentials.[8] On the basis of density functional theory (DFT) calculations, Nørskov and co-workers[9,10] identified a linear correlation between the binding energies of reaction intermediates on transition-metal surfaces, which dictates their electrocatalytic activity toward the eCO_2RR.[10] In this framework, the exceptional behavior of Cu in this reaction was rationalized by the mild adsorption energy of CO, which is a key reaction intermediate.[10] Nevertheless, pristine Cu electrodes show impractical overpotentials for the eCO_2RR and appreciable activity for the competing hydrogen evolution reaction (HER),[8,11,12] leading to poor selectivity. However, the aforementioned scaling relationship naturally constrains any performance optimization associated with simply tuning the electronic structure of the d-metal electrocatalysts. As a consequence, nonconventional approaches to break the scaling relationship are urgently required.

In this context, Kanan et al.[13] reported in 2012 that a Cu electrode derived from its oxide (oxide-derived copper; OD-Cu) exhibited improved performance toward CO and $HCOO^-$ at low overpotentials. The origin of such improvements is still under debate; claims on the active role of grain boundaries formed upon the reduction of copper oxide[13,14] contrast with persistent interstitial oxygen on the subsurface of OD-Cu positively modulating the electronic structure.[15,16] This finding opened up a new research direction targeting Cu-based

Received: September 15, 2017
Revised: November 17, 2017
Published: December 11, 2017

DOI: 10.1021/acscatal.7b03161
ACS Catal. 2018, 8, 837−844

materials modified with elements other than transition metals. In this respect, a successful modification of Cu with In[17,18] or Sn[19] was reported by Takanabe and co-workers, as reflected by Faradaic efficiencies (FEs) for CO greater than 90% at relatively small overpotentials (~400 mV). Later on, rationalization shed light on the complexity inherent to those systems.[20,21] p-Block modifiers are thought to participate in the formation of bonds on the surface according to theoretical studies, hence circumventing the scaling relationships.[22] Overall, these studies point to the potential of p-block elements as modifiers to tune the catalytic properties of Cu toward different eCO_2RR products.

From this standpoint, sulfur is an attractive candidate as a modifier due to its chemical similarities with oxygen. Herein, we describe the selective formation of formate over particulate sulfur-modified Cu (Cu−S) electrocatalysts prepared from sulfide precursors upon reductive reconstruction. The study of the influence of the particle size and sulfur content on the catalytic response unveiled a size−activity relationship correlating larger particle sizes with higher FEs to formate. Detailed characterization allowed us to gain insights on the catalytic role of sulfur, distribution, and chemical nature. In view of these results and the high practical relevance of formate as additive[23,24] and potential hydrogen carrier,[25−27] and its predicted leading role in breaking the barrier for eCO_2RR implementation,[28] we developed a targeted preparation route toward practical systems comprising submicron-sized Cu−S that indeed exhibited enhanced performance (>80% FEs at −0.8 V vs reversible hydrogen electrode; RHE), outperforming reported earth-abundant and cost-effective materials for formate production via the aqueous eCO_2RR.[6]

2. EXPERIMENTAL SECTION

2.1. Catalyst Preparation. Carbon-supported copper sulfide catalysts were prepared by wet chemistry under He atmosphere. Urea (200 mmol, Sigma-Aldrich, ≥ 99.5%) and appropriate amounts of thiourea (Sigma-Aldrich, > 95%), $Cu(NO_3)_2{\cdot}3H_2O$ (Sigma-Aldrich, ≥ 99.0%) and carbon black (Vulcan XC-72, Cabot Corporation) were first mixed in 18.2 MΩ cm ultrapure water (200 cm^3) at 298 K for 1 h. Equimolar amounts (0.05, 0.2, 0.5, and 2.0 mmol) of thiourea and copper nitrate were employed for preparing four different samples, denoted as CuS-1, -2, -3, and -4, respectively, while the amount of carbon black was varied to target a CuS loading of 5 wt % in each catalyst. The mixture was then heated to 363 K under vigorous stirring, kept at this temperature for 1 h, and then allowed to naturally cool to room temperature. The resulting mixture was washed with ultrapure water three times by centrifugation (6000 rpm, 10 min), and the obtained powders were dried under vacuum overnight at 353 K. Further details on the synthesis are provided in the Supporting Information (SI).

Unsupported bulk copper sulfide was prepared by a solvothermal route adopted from Wu et al.[21,29] Briefly, 4 mmol of $Cu(NO_3){\cdot}3H_2O$ and elemental sulfur (Sigma-Aldrich, > 95%) were mixed in 40 cm^3 of ethylene glycol (Sigma-Aldrich, 99%) at room temperature for >30 min. We carried out syntheses with different amounts of sulfur (0.016, 0.037, 0.066, 0.14, 0.63, and 6.5 mmol) to tune the sulfur content of the resulting materials. The mixture was then transferred into a 50 cm^3 Teflon-lined autoclave, and heat treated at 413 K for 12 h. The obtained mixture was washed and dried as described.

2.2. Electrode Preparation. The prepared electrocatalyst powders were deposited on a carbon gas diffusion layer (GDL) by airbrushing. A catalyst ink was prepared by dispersing the catalyst powder (50 mg) in a 1:1 mixture of ultrapure water (4 cm^3) and 2-propanol (4 cm^3, Sigma-Aldrich, 99.8%) to which Nafion solution (50 mm^3, 5 wt %, Sigma-Aldrich) was also added as a binder phase. The resulting mixture was sonicated for 15 min and then was sprayed onto the GDL (Sigracet 39BC, SGL Group) with an airbrush (Iwata Eclipse HP-SBS) at 353 K. A total powder loading of 1.5 mg cm^{-2} was typically achieved for each electrode.

2.3. Electrochemical Tests. A custom gastight glass cell with two compartments separated by a Nafion 212 membrane (Alfa Aesar, 0.05 mm thickness) was used for the electrochemical studies. Both chambers were filled with 40 cm^3 of a 0.1 M $KHCO_3$ solution (Sigma-Aldrich, 99.95% trace metals basis) prepared with ultrapure water. Before and during the measurement, CO_2 (Messer, purity 4.8) was supplied to the catholyte at a flow rate of 20 cm^3 min^{-1}, resulting in a pH of 6.7. A Pt wire and a Ag/AgCl (3.0 M KCl) were used as the counter and reference electrode, respectively. The working electrodes had a geometric area of ca. 1 cm^2, which was accurately quantified for each electrode with the ImageJ image processing and analysis software (Wayne Rasband, National Institutes of Health). All measurements were performed employing an Autolab PGSTAT302N potentiostat at room temperature. Current densities were normalized by the geometric surface area; and potentials were *iR* corrected (impedance spectroscopy, 100 kHz, 10 mV amplitude), and referenced to the reversible hydrogen electrode (RHE).

The double layer capacitance was measured by cyclic voltammograms (CV) in the potential range of open circuit potential ±15 mV at varying scan rates (2, 5, 10, 15, and 20 mV s^{-1}). The eCO_2RR performance was investigated by chronoamperometry (CA) for 1.5 h. Typically, the measurements were repeated several times. Averaged values are reported in this study. Gaseous products were analyzed using an online gas chromatograph (GC; SRI 8610C, Multi-Gas #3 configuration) with Ar as a carrier gas at a head pressure of 2.3 bar. Gas samples were injected and analyzed 10 min after the start of the electrolysis and thereafter every 15 min. The GC was equipped with a HayeSep D column and a Molecular Sieve 13X column. Liquid products were examined with a high-performance liquid chromatograph in a Merck LaChrom system equipped with a Bio-Rad Aminex HPX-87H column heated at 333 K and a refractive index detector (Hitachi Chromaster 5450), using 5 mM H_2SO_4 as eluent.

2.4. Catalyst Characterization. X-ray diffraction (XRD) patterns were obtained using a PANalytical X'Pert PRO-MPD diffractometer with Bragg−Brentano geometry using Ni-filtered Cu Kα radiation (λ = 0.1541 nm). The instrument was operated at 40 mA and 45 kV, and the patterns were recorded in the 10−70° 2θ range with an angular step size of 0.05° and a counting time of 180 s per step. The content of elements in the samples was quantified by X-ray fluorescence (XRF) spectroscopy using an Orbis Micro-XRF analyzer equipped with a 35 kV Rh anode and a silicon detector. The loading of copper in the supported catalyst was analyzed by inductively coupled plasma optical emission spectrometry (ICP-OES) using a Horiba Ultima 2 instrument. X-ray photoelectron spectroscopy (XPS) analysis was carried out with a PHI Quantum 2000 spectrometer (Physical Electronics) equipped with a 180° spherical capacitor energy analyzer, at a

DOI: 10.1021/acscatal.7b03161
ACS Catal. 2018, 8, 837−844

base pressure of 5×10^{-7} Pa using monochromatic Al Kα radiation (1486.68 eV). The binding energy scale was calibrated with the C 1s signal at 284.8 eV. Scanning electron microscopy (SEM) and backscattered electron (BSE) micrographs and energy dispersive X-ray (EDX) spectroscopy maps were acquired in a FEI Quanta 200F instrument. Powdered samples were dispersed in dry form onto fresh carbon paint deposited on an aluminum holder. In addition, scanning transmission electron microscopy (STEM) investigations combined with EDX mappings were performed in a FEI Talos F200X (high-brightness gun (XFEG)) at an accelerating voltage of 200 kV. STEM images (1024 × 1024 pixels) were recorded with a high-angle annular dark field (HAADF) detector at a frame rate of ca. 15 s. The selected imaging conditions give rise to atomic number (Z) contrast. Four silicon drift detectors attached to the Talos F200X microscope allowed for recording EDX maps with high signal/noise (S/N) ratio (measuring time: ca. 10 min) using the program Esprit 1.9 (Bruker).

3. RESULTS AND DISCUSSION

3.1. Nanosized CuS/C. Based on the potential similarities between the oxygen and sulfur modification of Cu-based eCO_2RR catalysts, we adopted a safe and potentially scalable approach (i.e., avoiding high-temperature treatments with H_2S) for the preparation of sulfur-modified Cu electrocatalysts in a practical form. To this end, size-controlled copper sulfide catalysts loaded on a carbon support (Vulcan XC-72) were prepared by a wet chemistry route. The XRD analysis (Figure 1a) of the catalysts showed diffraction peaks compatible with

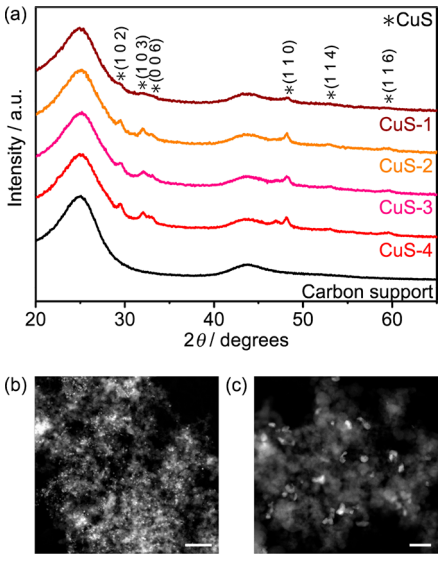

Figure 1. (a) X-ray diffraction (XRD) patterns of CuS-1 to CuS-4. Representative scanning transmission electron microscopy (STEM) images of CuS-3 in (b) wide and (c) magnified views. The XRD pattern of the carbon support is added as a reference. Scale bar: (b) 500 nm, (c) 100 nm.

stoichiometric CuS (except for one peak at 47° 2θ ascribable to $Cu_{1.8}S$), while such clear peaks were less defined for CuS-1 presumably due to its smaller size (vide infra), confirming the successful preparation of CuS. Additionally, STEM observations disclosed their nanometric nature. Figure 1b,c show representative STEM images (material shown: CuS-3, see SI Figure S1 for the other materials) exhibiting dispersed nanometer-sized particles on carbon black. An effective control of the particle size was achieved by varying the concentration of the copper and sulfur precursors in the synthesis protocol (SI Figure S2), as evidenced by a recognizable increase of the mean particle size in different samples (Table 1). The surface

Table 1. Minimum, Maximum, and Average Particle Sizes of Nanosized Cu−S Obtained from STEM Images

	size/nm		av size/nm			
sample	min	max	mean	50%	σ/−	Cu loading[a]/wt %
CuS-1	4	41	15	15	7	3.6
CuS-2	12	75	34	31	12	3.8
CuS-3	11	63	33	33	10	3.1
CuS-4	15	78	42	39	14	2.2

[a]Determined by inductively coupled plasma optical emission spectrometry.

state of the CuS/C catalysts was evaluated by XPS analysis of the corresponding electrodes. Spectra for CuS-1 and CuS-4 are presented in Figure 2 and in SI Figure S3. In the S 2p region (Figure 2a), the broad peak observed at 162.5 eV in both CuS-1 and CuS-4 is ascribable to any of the copper sulfide phases (i.e., Cu_2S or CuS).[30] In addition, the signal at higher binding energies can be assigned to sulfur species in Nafion (used as binder in the catalyst ink) as well as to sulfate species presumably formed by the oxidation of sulfides upon exposure to air.[31] In the Cu 2p region (Figure 2b), both samples exhibited a sharp peak centered at ca. 932 eV, which likely originated from contributions from two distinct Cu species: one from Cu^+ in Cu_2O (932.5 eV) accounting for more than half of the total area (ca. 55%, see spectral fitting in SI Figure S3), and the other at a lower binding energy (ca. 932 eV) ascribable to copper sulfides,[30] consistent with the S 2p spectra. There was no apparent contribution originating from CuO. To better elucidate the Cu state in the samples, the Auger emission (AE) spectra in the Cu LMM region were also analyzed (Figure 2c). Both CuS-1 and CuS-4 exhibited a signal centered at 917.5 eV, which indicates the presence of both Cu^+ (in Cu_2O and/or Cu_2S at 917 eV) and Cu^{2+} (in CuS at 918 eV) with a relatively similar composition.[30] Taken together, these observations suggest the formation of nanometrically shaped copper sulfide phase CuS, although the presence of metallic/oxidic Cu decorating the surface is plausible.

The catalytic performance of the CuS/C for the eCO_2RR was assessed by 1.5 h electrolyses in CO_2-saturated 0.1 M $KHCO_3$ (pH 6.7) at −0.6 and −0.8 V vs RHE (Figure 3). Carbon black (Vulcan XC-72) was chosen as the conductive support due to its almost inert catalytic nature (SI Figure S4). Remarkably, formate was observed as the main eCO_2RR product over all CuS/C catalysts, with only trace amounts of CO detected at −0.8 V vs RHE. Moreover, the FE to formate (FE_{HCOO^-}) as well as the current density increased almost monotonically from CuS-1 to CuS-4 at both potentials, accompanying the increase of the particle size.

Notably, CuS is not thermodynamically stable under the eCO_2RR conditions. Pourbaix diagrams[32] (SI Figure S5) clearly dictate an equilibrium potential for the CuS/Cu redox pair more positive than the applied working potentials (ca. −0.3 V compared to < −0.6 V vs RHE). Indeed, redox peaks ascribable to CuS/Cu were visible in the CVs prior to the reaction (SI Figure S6), confirming the reduction of CuS during the eCO_2RR. The reductive loss of CuS was also

DOI: 10.1021/acscatal.7b03161
ACS Catal. 2018, 8, 837−844

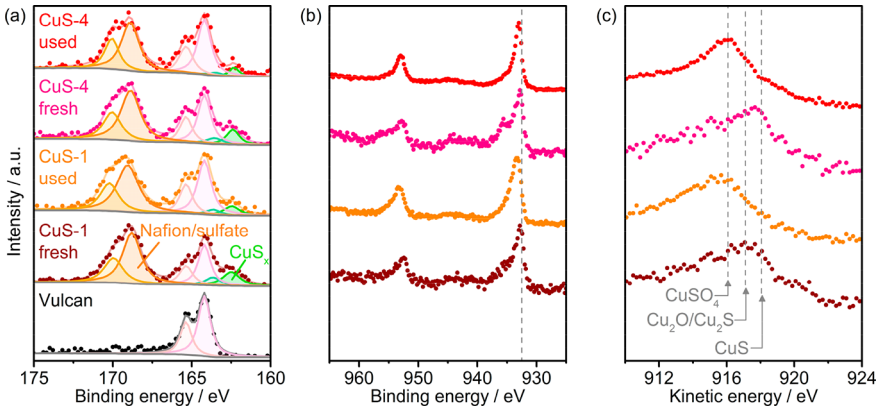

Figure 2. X-ray photoelectron spectroscopy (XPS) analysis and associated deconvolution in the (a) S 2p and (b) Cu 2p regions, and Auger emission (AE) spectra in the (c) Cu LMM region of CuS-1 and CuS-4 before and after the eCO_2RR test. The XPS spectrum of the carbon support (Vulcan XC-72) is included as a reference. The dashed vertical line in (b) is provided as a visual aid.

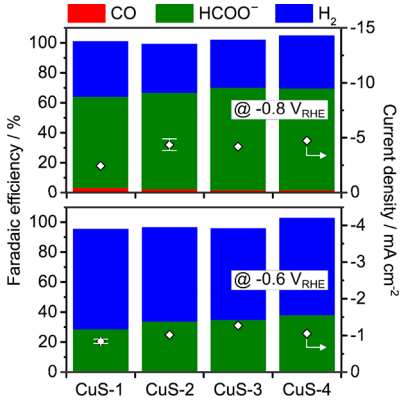

Figure 3. Faradaic efficiency (FE) and total current density over nanosized Cu−S catalysts. The data were obtained by chronoamperometry (CA) for 1.5 h, in 0.1 M $KHCO_3$ saturated with CO_2 (pH 6.7) at room temperature.

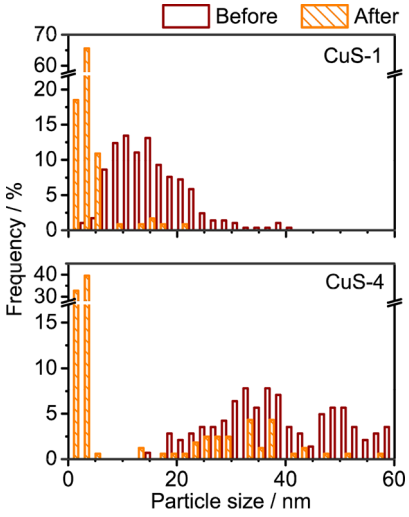

Figure 4. Particle size distribution obtained from STEM images for representative nanosized SD-Cu before and after the eCO_2RR test.

evidenced by XPS analysis. The spectra in the S 2p region (Figure 2a) revealed a considerable decrease of the relative area of the CuS peak (162.5 eV), which implies that most CuS phases present in the fresh sample were lost during eCO_2RR. Nevertheless, spectroscopic fingerprints compatible with sulfide phases remain detectable after the reaction, in marked contrast to OD-Cu, in which the Cu_2O phase is undetectable upon eCO_2RR.[13] In tandem, the Cu 2p region did not exhibit considerable changes (Figure 2b), presumably due to the almost identical binding energy for Cu_2O and copper sulfide. The presence of Cu_2O could be accounted for by the exposure of the samples to air.[21] Furthermore, the redox process was accompanied by a drastic structural reconstruction. Figure 4 presents the particle size distributions of the fresh and used samples. CuS-1 (initial size of 15 ± 7 nm) evolved toward an average particle size of ca. 3 nm after the electrochemical test. Similarly, the particle size of CuS-4 (ca. 42 nm) decreased to ca. 5 nm; nevertheless, relatively large particles (i.e., > 20 nm) persisted. Overall, these observations illuminated the drastic and presumably fast reductive reconstruction underwent by CuS-X materials upon exposure to the eCO_2RR operation conditions. The detected presence of a potentially persistent sulfide phase on the surface after prolonged operation and the plausible size-performance correlation observed uniquely shape this system and call for further fundamental studies and optimization strategies.

3.2. Solvothermally Prepared Cu−S Catalysts. Since the evaluation of the supported catalysts implied a positive correlation between the activity and selectivity for formate and the particle size, bulk S-modified materials were prepared with the aim of verifying this hypothesis and further improving the electrocatalytic performance toward formate while maintaining a powder form that can be readily applied to a practical electrode.[21,29] The sulfur content of the catalysts, expressed as the relative atomic ratio of sulfur S/(S + Cu), was tuned by varying the amount of the sulfur precursor in the solvothermal synthesis (Table 2). The size, morphology, and surface structure of the prepared samples were first studied by microscopy (Figure 5; also SI Figure S7) for representative samples with sulfur contents of 0.45 at% and 58.9 at%, denoted as L−S and H−S, respectively. SEM images disclosed a submicron-scale geometry, revealing that bulk materials were successfully obtained, whereas the corresponding EDX elemental maps exhibited 0.6 at% of sulfur in the L−S sample and 68.5 at% of homogeneously distributed sulfur in the H−S sample. SAED allowed phase identification by exposing diffraction rings indicative of polycrystalline Cu_2O in L−S and of CuS in H−S. Further insights on the bulk crystalline structure of the samples were elucidated by XRD analysis. The diffraction patterns shown in Figure 6a revealed that, below a

DOI: 10.1021/acscatal.7b03161
ACS Catal. 2018, 8, 837−844

Table 2. Quantity of Solid S Used during the Solvothermal Synthesis, the Corresponding Expected S Content, and the Actual S Content in the Resultant Samples Quantified by X-ray Fluorescence (XRF) Spectroscopy

quantity of solid S/mmol	expected S content/at%	actual S content/at%
0.016	0.4	0.007
0.037	0.9	0.009
0.067	1.6	0.45
0.14	3.3	1.8
0.63	13.7	13.1
6.5	61.8	58.9

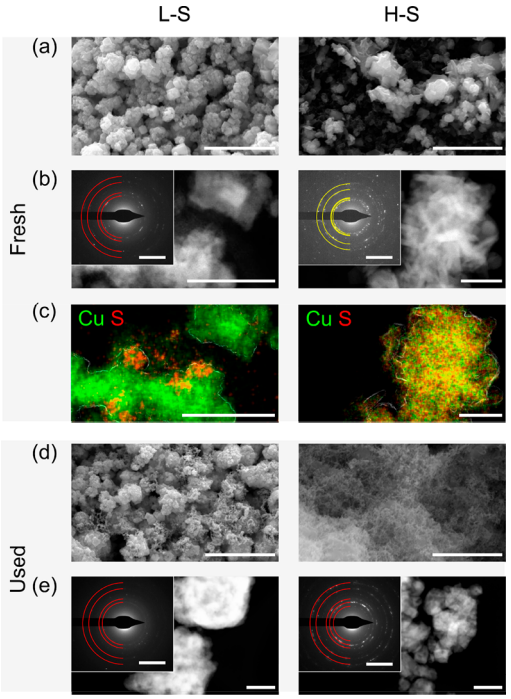

Figure 5. Micrographs of the solvothermally prepared samples: (a), (b), and (c) before, and (d) and (e) after the eCO_2RR test. (a) Scanning electron microscopy (SEM) images, (b) STEM images in high-angle annular dark field (HAADF) mode and selected area electron diffraction (SAED) in inset, (c) elemental maps obtained by energy-dispersive X-ray spectroscopy (EDX) corresponding to the STEM-HAADF images shown in (b), (d) SEM images, and (e) STEM-HAADF images and SAED patterns (inset). The yellow and red semicircles are overlaid over the diffraction rings corresponding to CuS and Cu_2O, respectively. White contours delimiting the edges of particles are superimposed as a visual aid in (c). Scale bar: (a) and (d) 2 μm; (b), (c), and (e) 200 nm; inset in (b) and (e) 5 1/nm.

sulfur content of 1.8 at%, Cu_2O was the main phase together with metallic Cu in the bulk structure. Associated with the increase of the sulfur content (13.3 at%), diffraction peaks from CuS were apparent in addition to the Cu_2O and Cu phases, and finally only peaks from CuS were observed at the highest sulfur content, thus coinciding with the surface crystal structure.

The surface chemical state of the materials was examined by XPS analysis (Figure 6, see SI for the details of the assignment of the spectra). In the S 2p region (Figure 6b), the spectroscopic evidence of sulfides was apparent in the H−S as reflected by the broad peak at ca. 162 eV, which could only be deconvoluted assuming contributions from both CuS and Cu_2S,[31] while the spectrum recorded from L−S essentially matched that of a sulfur-free sample. The XPS spectrum in the Cu 2p region and the Cu LMM Auger emission spectrum (Figure 6c and 6d, respectively; also see SI Figure S8) confirmed CuS as the major phase in the H−S sample, while the spectra from L−S and the sulfur-free samples were consistent with Cu_2O surfaces. Taken together, these results unequivocally associated low concentrations of the precursor with a S-modified copper oxide, whereas above a certain concentration threshold the formation of sulfide phases in the bulk was favored.

Figure 7 summarizes the eCO_2RR performance of the solvothermally prepared S-modified catalysts in CO_2 reduction electrolyses (1.5 h) at −0.6 V vs RHE (see also SI Figure S9 for the raw chronoamperometric profile). Trace amounts of incorporated sulfur (i.e., 0.007 at%) did not suppress the preference for the HER observed over the unmodified catalyst (i.e., FE_{H_2} of ca. 70%) although a suppression of CO and a favoring of formate as the main eCO_2RR product were already evidenced. In contrast, larger sulfur contents triggered a high selectivity toward formate (i.e., FE_{HCOO^-} higher than ca. 45%) and a current density of approximately 2.5 mA cm^{-2} which were practically independent of the sulfur content. It is interesting to note that the eCO_2RR performance observed over the (submicron-sized) solvothermally prepared Cu−S catalysts at −0.6 V was superior to that of the supported nanosized samples (i.e., FE_{HCOO^-} of ca. 50% vs less than 40%), which supports our hypothesis regarding the existence of a particle size effect in this class of Cu−S electrocatalysts.

After the electrochemical test, a surface roughening of the particles was apparent (Figure 5), consistent with the reconstruction observed on the nanosized Cu−S. Remarkably, both the L−S and H−S samples exhibited similar contents of sulfur following the electrolysis within the precision available to SEM-EDX quantification (i.e., 0.6 at% and 1.4 at%, respectively) in spite of the very large initial difference. This change was also evidenced by the disappearance of the characteristic features of the CuS/Cu redox couple in the CVs of the used samples (SI Figure S10). The SAED patterns in Figure 5e showed that the surface structure of both used samples comprised polycrystalline Cu_2O, which was presumably generated via the oxidation of metallic Cu that was formed under the cathodic conditions of eCO_2RR upon the exposure to air.[21] Interestingly, the presence of sulfides in both H−S and L−S samples after the electrolysis become highly plausible after XPS analysis (Figure 6b), although the high noise-to-signal ratio prevented reliable deconvolution in the latter case. Compared with the fresh material, the corresponding peak in H−S was shifted toward lower binding energies after the reaction, likely indicating the transformation of CuS into Cu_2S.[30] The corresponding analyses around Cu excitations (Figure 6c,d; also see SI Figure S8) showed Cu^+ as the predominant phase in both cases. Since the oxide phase was most likely formed upon the exposure of the sample to air,[21] these observations indicate that the cathodic environment of eCO_2RR induces the loss of excess sulfur in the catalysts and that the S-modified materials, irrespective of the initial sulfur content, attain a similar surface state under the eCO_2RR conditions, plausibly comprising Cu_2S and Cu as coexisting phases. Such a mechanism would explain the negligible impact of the initial sulfur content in the measured eCO_2RR performance of the catalysts. However, the observed preference for HER when only trace amounts of the modifier

DOI: 10.1021/acscatal.7b03161
ACS Catal. 2018, 8, 837−844

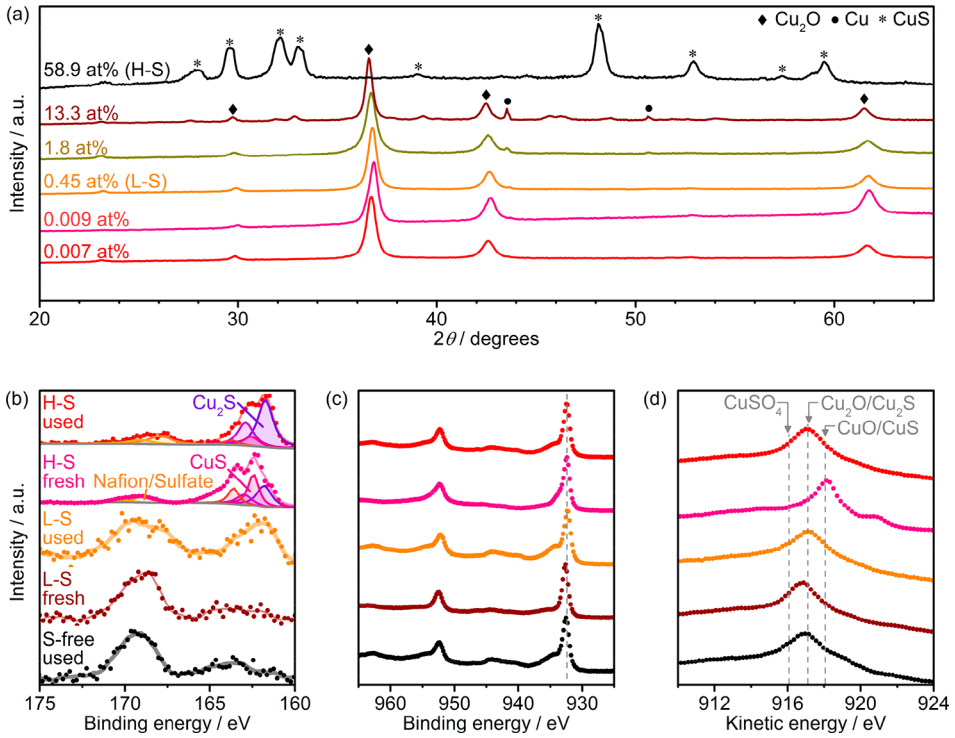

Figure 6. (a) XRD patterns of the solvothermally prepared samples. The sulfur content of the catalysts (defined as the relative atomic ratio of sulfur) as obtained by XRF is indicated. XPS spectra and associated deconvolution in the (b) S 2p and (c) Cu 2p regions, and AE spectra in the (d) Cu LMM region of H−S, L−S, and S-free samples before and after the eCO_2RR test. The dashed vertical lines in (b) and (c) are provided as a visual aid.

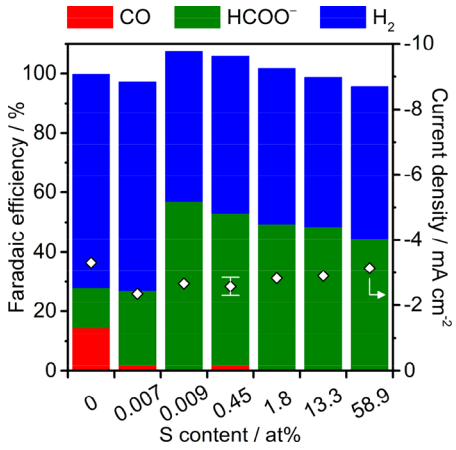

Figure 7. FE and total current density obtained over the solvothermally prepared samples. The data were obtained by CA at −0.6 vs RHE for 1.5 h, performed in 0.1 M $KHCO_3$ saturated with CO_2 (pH 6.7) at room temperature. The sulfur content determined by XRF spectroscopy is indicated in the figure.

are present suggests that there is a minimum required amount of sulfur to develop this catalytically advantageous surface configuration.

The Cu−S catalysts exclusively produce formate as has been described, which is in marked contrast with pristine Cu, which yields various products including formate, CO, hydrocarbons, and alcohols via eCO_2RR.[4,6,8,11] A plausible reaction mechanism over the pristine Cu surface was previously proposed on the basis of DFT calculations by Nørskov and co-workers:[9,10] CO_2 is first reduced into either *COOH or *OCHO intermediate species via one electron and proton transfer. Further reduction of *COOH generates *CO, which can either desorb as CO or experience successive reduction events leading to hydrocarbons and/or alcohols (CO path). On the other hand, *OCHO can be converted only into $HCOO^-$ upon further reduction ($HCOO^-$ path), which occurs in parallel to the CO path. Such a picture is well in line with the experimental studies,[4,33−35] and a recent report suggested its possible applicability to other metal surfaces.[12,36] Taking into consideration this reaction mechanism, the exclusive production of formate observed over the herein disclosed Cu−S electrocatalysts indicates that the modification of Cu with sulfur alters the energy levels of the corresponding key intermediate species (i.e., *COOH and *OCHO) and/or CO, leading to partial or complete deactivation of the CO path. Such a picture might be rationalized in a scenario where the binding energy of *OCHO over the Cu−S may be strengthened relative to the pristine Cu by the presence of positively charged Cu species, which would be stabilized by adjacent negatively charged sulfur, and thus binding CO_2 favorably through the relatively electronegative oxygen. In parallel, this surface configuration is expected to disfavor adsorption of CO_2 through the mildly electropositive carbon atom—as in the case of the *COOH intermediate—hence accounting for the absence of products associated with the CO path. Nonetheless, we anticipate that further elucidation of the intriguing reaction mechanism over the Cu−S electrocatalysts will require a combination of computational and spectroscopic studies guided by herein observed results.

On the basis of these findings, we further studied the eCO_2RR performance of the L−S sample as a representative case of Cu−S catalysts. Figure 8a shows the effect on the FE_{HCOO^-} of increasing the overpotential up to −0.9 V vs RHE,

DOI: 10.1021/acscatal.7b03161
ACS Catal. 2018, 8, 837−844

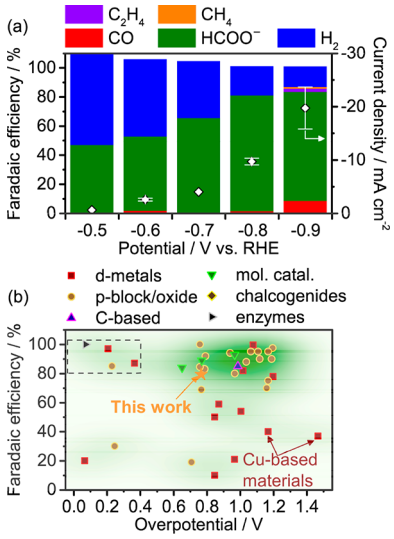

Figure 8. (a) FE and total current density as a function of applied potential over the L−S sample. The data were obtained by CA, performed in 0.1 M $KHCO_3$ saturated with CO_2 (pH 6.7) at room temperature. (b) FE against overpotential compiled from literature for different families of catalytic materials for the production of formate via eCO_2RR. The figure is adapted with permission from reference 6. Copyright 2017 American Chemical Society. Outstanding performances located at the left-top corner (designated with a dashed rectangle; FE > 80% and η < 0.40 V) were reported for nonscalable and/or cost-ineffective systems (see text).

at which the selectivity to formate drops due to the appearance of other eCO_2RR products. XPS analysis of the post reaction samples (SI Figure S11) disclosed the decrease in the relative intensity of the sulfide phase at more cathodic potentials, coinciding with the observed decrease of the FE toward formate. For the sake of comparison, the herein reported performance over Cu−S is plotted alongside other electrocatalysts that favor the production of formate (Figure 8b). For the production of formate, typical overpotentials (η) of at least 0.8 V are required to reach a FE higher than 80% using catalysts based on p-block elements, whereas the distinctive performance of Cu-based materials is centered at around 40% FE at η > 1.1 V. We note that outstanding values (FE > 80% and η < 0.40 V) are currently associated with cost-ineffective systems, such as atomically controlled structures,[37] precious metals,[38] or enzymes.[39] Further efforts have attempted to bring precious metal-based catalysts closer to practical requirements, for example, by improving their mass-activity by increasing their dispersion,[40,41] which is a key prerequisite[42] in these systems toward their implementation for the eCO_2RR. In contrast, the initially optimized Cu−S in this study achieved a Faradaic efficiency of 80% at an overpotential of 0.76 V, which locates it at the top of earth-abundant, cost-effective, and nontoxic electrocatalysts reported to date via aqueous eCO_2RR. In regard to stability, we note that the Cu−S catalyst sustained its exclusive formate production over 12 h of electrolysis at −0.8 V vs RHE, where a slight decrease in the average FE_{HCOO^-} of ca. 5% was observed (SI Figure S12a). Interestingly, the surface state did not change appreciably. The post reaction XPS analysis unveiled that the sulfide phase remained even after the long electrolysis (SI Figure S12b), indicating that the surface state comprising Cu_2S and Cu generated upon the initial rapid reconstruction event is stable within a range of potentials. Theoretical studies support the enhanced stability of Cu_2S on Cu with respect to its bulk state induced by the intergranular precipitation of Cu_2S in the Cu phase.[43] In this respect, the absence of any SAED patterns originating from such sulfide phases after the eCO_2RR test (Figure 5) suggests the presence of small quantity of Cu_2S and/or its amorphous nature, which hampers unambiguous elucidation of the active phase at this stage and calls for further investigation. All in all, this study demonstrated the selective production of formate via aqueous eCO_2RR over sulfur-modified Cu electrocatalysts, adding an advantageous candidate to Cu-based electrocatalysts for this reaction.[17−22,44−47]

4. CONCLUSIONS

Copper-based electrocatalysts modified with sulfur were studied for CO_2 reduction in aqueous media. Size-controlled carbon-supported nanometric CuS catalysts were successfully synthesized by a wet chemistry approach. These catalysts selectively produced formate with only trace amounts of CO at moderate overpotential (e.g., FE_{HCOO^-} > 60% at −0.8 V vs RHE). A rapid and drastic reconstruction toward smaller particles, provoked by the reduction of the CuS phases, took place on the CuS particles under operation conditions, thus leading to the formation of sulfur-modified Cu as the material accounting for the observed electrocatalytic activity. The selectivity to formate was positively correlated with increasing initial particle sizes, which, in turn, favored the survival of larger particles (e.g., > 20 nm) during the in situ reconstruction. A detectable amount of sulfur remained in the Cu matrix upon reaction in all cases. Bearing in mind the plausible size−activity relationship, submicron-sized Cu−S catalysts were prepared via a solvothermal route that allowed the variation of the sulfur content. With increasing sulfur content, both the bulk and surface structure of the solvothermally prepared catalysts evolved from Cu_2O to CuS. Nevertheless, the reaction rate and FE_{HCOO^-} were found to be mostly insensitive to the initial sulfur content above a certain trace level, which was accounted for by the fact that the catalysts attained a similar surface configuration under the cathodic reaction conditions of the eCO_2RR. The solvothermally prepared electrocatalysts exhibited improved FEs to formate (ca. 80% at −0.8 V vs RHE) compared with the nanometric CuS materials, and they sustained their high selectivity over 12 h. Overall, these findings open up new perspectives for Cu-based materials in the eCO_2RR and provide a solid understanding of the basic characteristics shaping the behavior of Cu−-S catalysts, thus offering a valuable platform for gaining further fundamental insights leading to improved kinetics toward formate. At this stage, the developed Cu−S sits at the top of reported performance for practical, cost-effective, and earth-abundant catalysts toward the electrocatalytic production of formate via aqueous eCO_2RR.

■ ASSOCIATED CONTENT

Supporting Information

The Supporting Information is available free of charge on the ACS Publications website at DOI: 10.1021/acscatal.7b03161.

Procedure for the calculation of Faradaic efficiency of the gas and liquid products, synthesis details and characterization of copper-based catalysts, and calculated Pourbaix diagrams for copper species (PDF)

DOI: 10.1021/acscatal.7b03161
ACS Catal. 2018, 8, 837−844

AUTHOR INFORMATION

Corresponding Author

*Phone: +41 44 633 7120. E-mail: jpr@chem.ethz.ch.

ORCID

Gastón O. Larrazábal: 0000-0003-4218-3514

Javier Pérez-Ramírez: 0000-0002-5805-7355

Notes

The authors declare no competing financial interest.

ACKNOWLEDGMENTS

This work was sponsored by the European Union under the a-leaf project (732840-A-LEAF) and by ETH Zurich (Research Grant ETH-01 14-1). Evgeniya Vorobyeva is kindly acknowledged for TEM analyses. The authors acknowledge the Scientific Center for Optical and Electron Microscopy (ScopeM) of ETH Zurich for access to its facilities.

REFERENCES

(1) Seh, Z. W.; Kibsgaard, J.; Dickens, C. F.; Chorkendorff, I.; Nørskov, J. K.; Jaramillo, T. F. *Science* **2017**, *355*, eaad4998.

(2) Montoya, J. H.; Seitz, L. C.; Chakthranont, P.; Vojvodic, A.; Jaramillo, T. F.; Nørskov, J. K. *Nat. Mater.* **2017**, *16*, 70−81.

(3) Vayens, C. G.; White, R. E.; Gamboa-Aldeco, M. E. *Modern Aspects of Electrochemistry*; Springer: New York, 2008; Vol. *42*, pp 89−189.

(4) Kortlever, R.; Shen, J.; Schouten, K. J. P.; Calle-Vallejo, F.; Koper, M. T. M. *J. Phys. Chem. Lett.* **2015**, *6*, 4073−4082.

(5) Martín, A. J.; Larrazábal, G. O.; Pérez-Ramírez, J. *Green Chem.* **2015**, *17*, 5114−5130.

(6) Larrazábal, G. O.; Martín, A. J.; Pérez-Ramírez, J. *J. Phys. Chem. Lett.* **2017**, *8*, 3933−3944. Further permissions related to the material excerpted should be directed to the ACS.

(7) Hori, Y.; Kikuchi, K.; Suzuki, S. *Chem. Lett.* **1985**, *14*, 1695−1698.

(8) Hori, Y.; Wakebe, H.; Tsukamoto, T.; Koga, O. *Electrochim. Acta* **1994**, *39*, 1833−1839.

(9) Peterson, A. A.; Abild-Pedersen, F.; Studt, F.; Rossmeisl, J.; Nørskov, J. K. *Energy Environ. Sci.* **2010**, *3*, 1311−1315.

(10) Peterson, A. A.; Nørskov, J. K. *J. Phys. Chem. Lett.* **2012**, *3*, 251−258.

(11) Kuhl, K. P.; Cave, E. R.; Abram, D. N.; Jaramillo, T. F. *Energy Environ. Sci.* **2012**, *5*, 7050−7059.

(12) Kuhl, K. P.; Hatsukade, T.; Cave, E. R.; Abram, D. N.; Kibsgaard, J.; Jaramillo, T. F. *J. Am. Chem. Soc.* **2014**, *136*, 14107−14113.

(13) Li, C. W.; Kanan, M. W. *J. Am. Chem. Soc.* **2012**, *134*, 7231−7234.

(14) Verdaguer-Casadevall, A.; Li, C. W.; Johansson, T. P.; Scott, S. B.; McKeown, J. T.; Kumar, M.; Stephens, I. E. L.; Kanan, M. W.; Chorkendorff, I. *J. Am. Chem. Soc.* **2015**, *137*, 9808−9811.

(15) Mistry, H.; Varela, A. S.; Bonifacio, C. S.; Zegkinoglou, I.; Sinev, I.; Choi, Y.-W.; Kisslinger, K.; Stach, E. A.; Yang, J. C.; Strasser, P.; Cuenya, B. P. *Nat. Commun.* **2016**, *7*, 12123.

(16) Eilert, A.; Cavalca, F.; Roberts, F. S.; Osterwalder, J.; Liu, C.; Favaro, M.; Crumlin, E. J.; Ogasawara, H.; Friebel, D.; Pettersson, L. G. M.; Nilsson, A. *J. Phys. Chem. Lett.* **2017**, *8*, 285−290.

(17) Rasul, S.; Anjum, D. H.; Jedidi, A.; Minenkov, Y.; Cavallo, L.; Takanabe, K. *Angew. Chem., Int. Ed.* **2015**, *54*, 2146−2150.

(18) Jedidi, A.; Rasul, S.; Masih, D.; Cavallo, L.; Takanabe, K. *J. Mater. Chem. A* **2015**, *3*, 19085−19092.

(19) Sarfraz, S.; Garcia-Esparza, A. T.; Jedidi, A.; Cavallo, L.; Takanabe, K. *ACS Catal.* **2016**, *6*, 2842−2851.

(20) Larrazábal, G. O.; Martín, A. J.; Mitchell, S.; Hauert, R.; Pérez-Ramírez, J. *ACS Catal.* **2016**, *6*, 6265−6574.

(21) Larrazábal, G. O.; Martín, A. J.; Krumeich, F.; Hauert, R.; Pérez-Ramírez, J. *ChemSusChem* **2017**, *10*, 1255−1265.

(22) Shin, H.; Ha, Y.; Kim, H. *J. Phys. Chem. Lett.* **2016**, *7*, 4124−4129.

(23) Hietala, J.; Vuori, A.; Johnsson, P.; Pollari, I.; Reutemann, W.; Kieczka, H. Formic Acid. *Ullmann's Encyclopedia of Industrial Chemistry*; John Wiley & Sons, Inc: Hoboken, NJ, 2016; pp 1−22.

(24) Gibson, H. W. *Chem. Rev.* **1969**, *69*, 673−692.

(25) Rice, C.; Ha, S.; Masel, R. I.; Waszczuk, P.; Wieckowski, A.; Barnard, T. *J. Power Sources* **2002**, *111*, 83−89.

(26) Yu, X.; Pickup, P. G. *J. Power Sources* **2008**, *182*, 124−132.

(27) Yan, B.; Concannon, N. M.; Milshtein, J. D.; Brushett, F. R.; Surendranath, Y. *Angew. Chem., Int. Ed.* **2017**, *56*, 7496−7499.

(28) Sternberg, A.; Jens, C. M.; Bardow, A. *Green Chem.* **2017**, *19*, 2244−2259.

(29) Wu, C.; Yu, S.-H.; Antonietti, M. *Chem. Mater.* **2006**, *18*, 3599−3601.

(30) NIST X-ray Photoelectron Spectroscopy Database. *X-ray Photoelectron Spectroscopy Database 20, Version 4.1*; National Institute of Standards and Technology: Gaithersburg, 2012; See the following: http://srdata.nist.gov/xps/ (Accessed December 21, 2017).

(31) Kundu, M.; Hasegawa, T.; Terabe, K.; Yamamoto, K.; Aono, M. *Sci. Technol. Adv. Mater.* **2008**, *9*, 035011.

(32) Haynes, W. M.; Lide, D. R. *Handbook of Chemistry and Physics*, 92nd ed., CRC Press: Boca Raton, FL, 2011; pp 5-11, 5-41, 5-66, 5-67.

(33) Hori, Y.; Murata, A.; Takahashi, R.; Suzuki, S. *J. Am. Chem. Soc.* **1987**, *109*, 5022−5023.

(34) Cook, R. L.; MacDuff, R. C.; Sammells, A. F. *J. Electrochem. Soc.* **1989**, *136*, 1982−1984.

(35) Hori, Y.; Murata, A.; Takahashi, R. *J. Chem. Soc., Faraday Trans. 1* **1989**, *85*, 2309−2326.

(36) Feaster, J. T.; Shi, C.; Cave, E. R.; Hatsukade, T.; Abram, D. N.; Kuhl, K. P.; Hahn, C.; Nørskov, J. K.; Jaramillo, T. F. *ACS Catal.* **2017**, *7*, 4822−4827.

(37) Gao, S.; Lin, Y.; Jiao, X.; Sun, Y.; Luo, Q.; Zhang, W.; Li, D.; Yang, J.; Xie, Y. *Nature* **2016**, *529*, 68−71.

(38) Kortlever, R.; Peters, I.; Koper, S.; Koper, M. T. M. *ACS Catal.* **2015**, *5*, 3916−3923.

(39) Reda, T.; Plugge, C. M.; Abram, N. J.; Hirst, J. *Proc. Natl. Acad. Sci. U. S. A.* **2008**, *105*, 10654−10658.

(40) Min, X.; Kanan, M. W. *J. Am. Chem. Soc.* **2015**, *137*, 4701−4708.

(41) Rahaman, M.; Dutta, A.; Broekmann, P. *ChemSusChem* **2017**, *10*, 1733−1741.

(42) Verma, S.; Kim, B.; Jhong, H.-R.; Ma, S.; Kenis, P. J. A. *ChemSusChem* **2016**, *9*, 1972−1979.

(43) Korzhavyi, P. A.; Abrikosov, I. A.; Johansson, B. *Acta Mater.* **1999**, *47*, 1417−1424.

(44) Hoffman, Z. B.; Gray, T. S.; Moraveck, K. B.; Gunnoe, T. B.; Zangari, G. *ACS Catal.* **2017**, *7*, 5381−5390.

(45) Li, Q.; Fu, J.; Zhu, W.; Chen, Z.; Shen, B.; Wu, L.; Xi, Z.; Wang, T.; Lu, G.; Zhu, J.-J.; Sun, S. *J. Am. Chem. Soc.* **2017**, *139*, 4290−4293.

(46) Huang, Y.; Deng, Y.; Handoko, A.; Goh, G. K. L.; Yeo, B. S. *ChemSusChem*, **2017**, DOI: 10.1002/cssc.201701314.

(47) Lv, W.; Zhou, J.; Bei, J.; Zhang, R.; Wang, L.; Xu, Q.; Wang, W. *Appl. Surf. Sci.* **2017**, *393*, 191−196.

DOI: 10.1021/acscatal.7b03161
ACS Catal. 2018, 8, 837−844